Emulating Human Kinematic Behavior on Lower-Limb Prostheses via Multi-Contact Models and Force-Based Nonlinear Control

Rachel Gehlhar and Aaron D. Ames

Abstract—Active lower-limb prostheses could enable more natural assisted locomotion by contributing net positive work through important gait events, such as ankle push-off. This paper uses multi-contact models of locomotion together with force-based nonlinear optimization-based controllers to achieve human-like kinematic behavior, including ankle push-off, on a powered transfemoral prosthesis. In particular, we leverage model-based control approaches for dynamic bipedal robotic walking to develop a systematic method to realize human-like walking on a powered prosthesis that does not require subjectspecific tuning. The proposed controller is implemented on a prosthesis for 2 subjects without tuning between subjects, emulating subject-specific human kinematic trends on the prosthesis joints. These experimental results demonstrate that our forcebased nonlinear control approach achieves better tracking of human-like kinematic trajectories, with an average RMSE of 0.0223 during weight-bearing, compared to 2 non-force-sensing methods with an average RMSE of 0.0411 and 0.0430.

I. Introduction

In human walking, ankles contribute the most positive work of trailing leg joints in forward rocking [1] and contribute up to 60% of the total energy generated by a limb during a gait cycle [2]. Ankle push-off specifically contributes to the forward acceleration of the body [3] and also greatly smooths the transition from double support to swing phase in human gait [4]. Researchers showed for a simple powered walking model, that toe push-off can supply energy to the system at a quarter of the cost of applying a hip torque because this toe push-off reduces the collision energy loss at heel strike [5]. For amputees specifically, increasing prosthetic ankle push-off can reduce the loading impulse of the intact limb and the risk of knee osteoarthritis for amputees [6]. While the importance of an ankle that can generate net positive work is clear, especially for amputees, current commercially available devices for amputees remain mostly limited to passive devices. Additionally, for powered prostheses, controlling ankle actuators to produce natural and dynamic walking has proven challenging.

Lower-limb passive prostheses cannot contribute net positive work to a human the way muscles do [7]. Amputees walking with these devices expend more energy in walking, exhibit a decrease in comfortable walking speed, and have shorter step length [8], [9]. Powered prostheses can generate net positive work, but require a control strategy. One of the

*This material is based upon work supported by NSF Awards 1923239 and 1924526, and Wandercraft under Award No. WANDERCRAFT.21. This research was approved by California Institute of Technology Institutional Review Board with protocol no. 21-0693 for human subject testing.

R. Gehlhar and A. Ames are with the Department of Mechanical and Civil Engineering, California Institute of Technology, Pasadena, CA 91125 USA. Emails: {rgehlhar, ames}@caltech.edu



Fig. 1. (top) Subject 1 and (bottom) Subject 2 walking with powered prosthesis controlled by multi-domain model-based prosthesis controller with real-time force sensing following provably stable human-like walking trajectories. Labels indicate the respective domain the human-prosthesis is in in the multi-domain hybrid-system graph shown in Fig. 2

most commonly used control methods for these devices is impedance control [10]–[12], which divides the gait cycle into multiple discrete phases and tunes impedance parameters for each phase. This process takes hours to tune [13] to achieve human-like walking behavior [14] and needs to be repeated for every subject and behavior. Given there are over 600,000 lower-limb amputees in the US alone [15], it is not feasible to conduct this process for every potential user.

With the goal of developing a more systematic method to construct controllers for powered prostheses, we look to model-based control methods developed for bipedal robots that generate stable walking trajectories offline [16]-[18]. The hybrid zero dynamics (HZD) framework [19] used by these methods accounts for the impact dynamics present in walking at foot strike and the zero dynamics that occur from underactuation. This framework also allows modeling of multiple domains of continuous dynamics and the discrete connections between them as encoded by a directed cycle. This multi-domain hybrid system can model multi-contact behavior, such as the changing contacts of heel-toe roll used for ankle push-off, and can be used to generate trajectories that satisfy formal guarantees of stability. By tracking these trajectories online through a model-independent method, the end result has been multi-contact walking on bipedal robots [18], [20] and a powered prosthesis [21].

In order to retain stability guarantees online, control Lyapunov functions (CLFs) were employed in a quadratic program (QP) on bipedal robots [22], [23]. CLFs require knowledge of the full-order dynamics which is unavailable on a prosthesis since the human dynamics are unknown. Previous work developed a separable subsystem framework [24], [25] and proved that signals from an inertial measurement

unit (IMU) and a load cell at the socket interface could complete the prosthesis model and a class of prosthesis subsystem controllers could guarantee full-order system stability [26].

This paper implements a controller of the class in [26] to realize multi-contact behavior on a prosthesis tracking human-like trajectories generated through HZD methods. This paper differs from [21] in both method and results, using a formally grounded force-based controller to achieve human-like walking, verified through the kinematics. The work of [27] realized the first model-based lower-limb prosthesis controller with real-time force sensing on the knee of a powered prosthesis in 2 phases, stance and swing, with 1 prescribed walking gait. This paper extends the work of [27] in 3 major ways:

- we simultaneously apply the first model-based lowerlimb prosthesis controller with real-time force sensing to the ankle in addition to the knee of a transfemoral prosthesis,
- 2) we expand this model-based controller to a 6-domain hybrid system framework to emulate human multicontact behavior (heel-toe roll),
- 3) we demonstrate this new controller on 2 subjects with 2 different subject-specific prescribed walking gaits, and compare it to 2 other control methods.

This paper overviews the multi-domain hybrid system used to model multi-contact behavior and presents the system dynamics used to model the human and prosthesis in Section II. Section III describes the separable output functions we use to construct a controller for the prosthesis. This section also covers the trajectory generation method that aims to match human kinematic data while also satisfying stability guarantees for the human-prosthesis system. To implement these trajectories, we construct our control method in Section IV. In Section V, we describe the powered prosthesis platform on which we implement the controller. We realize this controller on 2 subjects and present the resultant human-like joint trajectories of the prosthesis along with comparisons to 2 other tested control methods. Finally, we discuss future directions in Section VI.

II. HUMAN-PROSTHESIS MULTI-DOMAIN MODEL

To model the multi-contact behavior of human walking, we use a multi-domain hybrid system model. To obtain the dynamics for this system, we model the human-prosthesis system as a walking robot.

Multi-Domain Hybrid System. We consider 3 phases per step for human walking: heel strike (hs) when the swinging foot's heel reaches the ground, toe strike (ts) when that foot's toe reaches the ground, and heel lift (hl) when the other foot's heel lifts off of the ground and becomes the swinging leg. We omit a fourth phase of the toe lifting between toe strike and heel lift because it is a very short phase. Since a human walking with a prosthesis is an asymmetric system, we consider separate phases for the right and left leg, prefacing the abbreviations with "r" and "l" respectively, giving a total of 6 phases. The current phase of the system is dictated by the

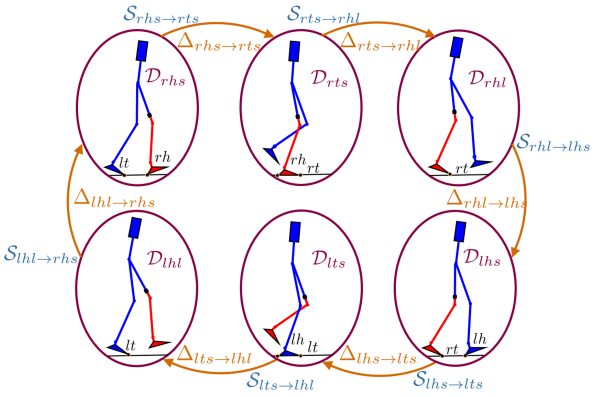


Fig. 2. Six-domain directed graph of human-prosthesis hybrid system, modeling respective foot contact points for different phases of walking.

foot contacts present. The set of all contact points is given by $\mathcal{C} = \{rh, rt, lh, lt\}$ signifying the right heel, right toe, left heel, and left toe, respectively. Fig. 2 shows the contact points present for each phase, or *domain*, of walking.

To account for the impact dynamics that occur when a foot strikes the ground in walking, we model the human-prosthesis system as a hybrid system. This *multi-domain hybrid control system* is defined as a tuple [20], [28]:

$$\mathscr{H}\mathscr{C} = (\Gamma, \mathcal{D}, \mathcal{U}, S, \Delta, FG),$$

where:

- $\Gamma = (V, E)$ is a directed cycle, with vertices $V = \{rhs, rts, rhl, lhs, ltl, lhl\}$ and edges $E = \{e = \{v \to v^+\}\}|_{v \in V}$, where v^+ is the subsequent vertex of v in the directed graph;
- $\mathcal{D} = \{\mathcal{D}_v\}|_{v \in V}$, set of *domains of admissibility*, meaning a set of physically feasible states;
- $\mathcal{U} = \{u_v\}|_{v \in V}$, set of admissible *control inputs*;
- $S = \{S_e\}|_{e \in E}$, set of guards or switching surfaces, with $S_e \subset \mathcal{D}_v$, that are transition points between one domain, \mathcal{D}_v , and the next, \mathcal{D}_{v^+} , in the directed cycle;
- $\Delta = \{\Delta_e\}|_{e \in E}$, set of *reset maps*, $\Delta_e : S_e \subset \mathcal{D}_v \to \mathcal{D}_{v^+}$, that define the discrete transitions triggered at S_e , giving the postimpact states of the system: $x^+ = \Delta_e(x)$, where $x \in \mathcal{D}_v$ and $x^+ \in \mathcal{D}_{v^+}$;
- $FG = \{(f_v, g_v)\}_{v \in V}$ with (f_v, g_v) , a control system on \mathcal{D}_v , that defines the continuous dynamics $\dot{x} = f_v(x) + g_v(x)u_v$ for each $x \in \mathcal{D}_v$ and $u_v \in \mathcal{U}$.

Human-Prosthesis Model. To define a control system for a human wearing a prosthesis, we model this human-prosthesis system as a series of 8 rigid links and 12 joints in 2D space, shown in Fig. 3. We define these 12 DOFs by configuration coordinates $q=(q_l^T,q_f^T,q_p^T)^T\in\mathbb{R}^{12}$ which define configuration space \mathcal{Q} . Here $q_l\in\mathbb{R}^7$ represents the coordinates of the human, including the floating base coordinates $q_B\in\mathbb{R}^3$; $q_f\in\mathbb{R}^3$ is the x and z Cartesian position and pitch of the fixed joint that connects the human to the prosthesis at the socket; and $q_p\in\mathbb{R}^2$ represents the prosthesis subsystem coordinates. We have $m_r=4$ available actuators for the human and $m_s=2$ for the prosthesis, meaning all joints that are not fixed or a floating base are actuated. The following Euler-Lagrange equation gives the

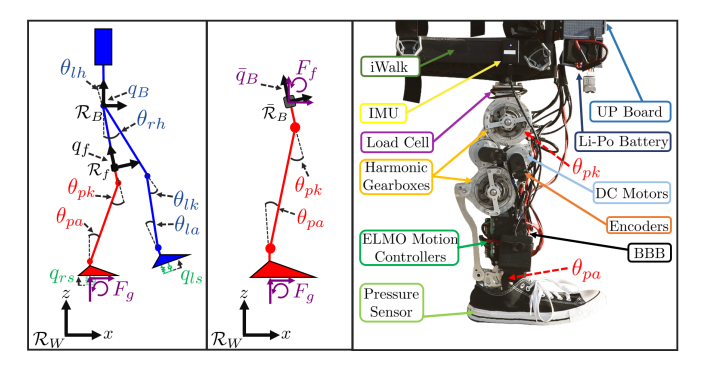


Fig. 3. (left) Human-prosthesis model with the prosthesis subsystem and coordinates in red, the human remaining system and coordinates in blue, and the ground model and coordinates in green. (middle) The equivalent prosthesis subsystem modeled with its own base coordinates \bar{q}_B and fixed joint forces F_f . (right) Powered prosthesis platform AMPRO3 labeled with subsystem coordinates and hardware component names.

constrained dynamics [29],

$$D(q)\ddot{q} + H(q, \dot{q}) = B_v u_v + J_{h,v}^T(q) \lambda_{h,v}$$
(1)

$$J_{h,v}(q)\ddot{q} + \dot{J}_{h,v}(q, \dot{q})\dot{q} = 0.$$

where D(q) is the inertia matrix; $H(q,\dot{q})$ contains the centrifugal, Coriolis, and gravity terms; B_v is the domain dependent actuation matrix, u_v is the control input for \mathcal{D}_v , and $J_{h,v}(q)$ is the Jacobian of the holonomic constraints $h_v(q)$ for the contact points in \mathcal{D}_v . This Jacobian projects the ground reaction forces (GRFs) $\lambda_{h,v}$.

We compute human model parameters by using human inertia, limb mass, and limb length percentage data from [30], [31] and a given subject's weight, height, and sex. We obtain model parameters of our powered prosthesis, AMPRO3 [32], from a CAD model.

Prosthesis Subsystem. To implement a model-based prosthesis controller, we require a model with states and inputs that can be measured on-board. Using a floating base with coordinates \bar{q}_B at the human-prosthesis interface, we have configuration coordinates $\bar{q} = (\bar{q}_B^T, q_p^T)^T$, shown in Fig. 3. The dynamics for this robotic subsystem are,

$$\bar{D}(\bar{q})\ddot{\bar{q}} + \bar{H}(\bar{q}, \dot{\bar{q}}) = \bar{B}_v u_{s,v} + \bar{J}_{h,v}^T(\bar{q}) \bar{\lambda}_{h,v} + \bar{J}_f^T(\bar{q}) F_f \quad (2)$$

$$\bar{J}_{h,v}(\bar{q}) \ddot{\bar{q}} + \dot{\bar{J}}_{h,v}(\bar{q}, \dot{\bar{q}}) \dot{\bar{q}} = 0, \quad (3)$$

including the interaction forces F_f it experiences with the human at the fixed joint and its projection J_f . The base coordinates \bar{q}_B and their velocities $\dot{\bar{q}}$ are measured by an IMU. The interaction forces F_f are measured by a load cell at the socket interface, the vertical force and pitch moment components of $\bar{\lambda}_{h,v}$ are measured by an insole pressure sensor, and the horizontal component of $\bar{\lambda}_{h,v}$ can be calculated by solving for \ddot{q} in the dynamics (2) and substituting it into the holonomic constraint equation (3):

$$\bar{\lambda}_{h,v} = (\bar{J}_{h,v}\bar{D}^{-1}\bar{J}_{h,v}^T)^{-1}(\bar{J}_{h,v}\bar{D}^{-1}(\bar{H} - \bar{B}_v u_{s,v} - \bar{J}_f^T F_f) - \dot{\bar{J}}_{h,v}\dot{q}),$$

where we now drop the arguments for notational simplicity. **Compliant Ground Model.** To account for the compliance the prosthesis foot and human foot experience in ground contact with their shoes, we include a spring-damper at the base of each foot in our robot model to serve as a "ground

model". We use a spring stiffness of 60,000N/m and a damping coefficient of 600Ns/m [33], [34]. These prismatic joints have coordinates q_{rs} and q_{ls} for the right and left spring, respectively. This allows us to generate model-based trajectories with more realistic impact dynamics. Since on hardware the prosthesis is measuring the forces at the level of the shoe insole, instead of the forces beneath the shoe, we do not include this ground model in our prosthesis subsystem.

Nonlinear Control System. We form the full-order robotic dynamic system (1) into a nonlinear control system ODE with states $x_q = (q^T, \dot{q}^T)^T$:

$$\dot{x}_{q} = \underbrace{\begin{bmatrix} \dot{q} \\ D^{-1}(-H + J_{h,v}^{T} \lambda_{h,v}) \end{bmatrix}}_{f_{q,v}(x_{q})} + \underbrace{\begin{bmatrix} 0 \\ D^{-1} B_{v} \end{bmatrix}}_{g_{q,v}(x_{q})} u_{v}. \tag{4}$$

By rearranging the states as $x=(x_r^T,x_s^T)^T$, with $x_r=(q_l^T,q_f^T,\dot{q}_l^T,\dot{q}_f^T)^T$ and $x_s=(q_p^T,\dot{q}_p^T)^T$, we obtain a control system of this form [24]:

$$\begin{bmatrix} \dot{x}_r \\ \dot{x}_s \end{bmatrix} = \underbrace{\begin{bmatrix} f_v^r(x) \\ f_v^s(x) \end{bmatrix}}_{f_v(x)} + \underbrace{\begin{bmatrix} g_{1,v}^r(x) & g_{2,v}^r(x) \\ 0 & g_v^s(x) \end{bmatrix}}_{g_v(x)} \begin{bmatrix} u_{r,v} \\ u_{s,v} \end{bmatrix},$$

$$x_v \in \mathbb{R}^{n_r}, x_s \in \mathbb{R}^{n_s}, u_{r,v} \in \mathbb{R}^{m_{r,v}}, u_{s,v} \in \mathbb{R}^{m_s}.$$

We consider the bottom row of this matrix to be the *separable subsystem* and the top row to be the *remaining system* [24], [25]. This form shows the dynamics of x_s do not depend on inputs $u_{r,v}$, allowing us to construct model-based controllers for subsystem outputs independent of the remaining system. While this subsystem depends on full-system states, we obtain an *equivalent subsystem* by the same ODE transformation used for (4):

$$\dot{x}_s = \bar{f}^s(\mathcal{X}) + \bar{g}^s(\mathcal{X})u_s,$$

$$\mathcal{X} = (\bar{x}_r^T, x_s^T, F_f^T)^T \in \mathbb{R}^{\bar{n}}.$$
(5)

Here $\bar{x}_r=(\bar{q}_B^T, \dot{\bar{q}}_B^T)^T$ are measurable states. For this robotic system form, a transformation T exists such that $T(x)=\mathcal{X}$ and $\bar{f}_v^s(\mathcal{X})=f_v^s(x)$ and $\bar{g}_v^s(\mathcal{X})=g_v^s(x)$ for all x [24]. With an IMU and load cell to complete the model, we can now develop model-based controllers for the prosthesis subsystem based solely on the prosthesis model and locally available sensory information.

III. GENERATING SUBJECT-SPECIFIC HUMAN-INSPIRED WALKING TRAJECTORIES

To develop a model-based controller for the prosthesis, we start by constructing outputs for the entire human-prosthesis system such that we can generate prosthesis trajectories that are provably stable with a human model. To generate trajectories that both emulate human kinematic behavior and are provably stable for a human model walking with a powered prosthesis, we included human motion capture data in a hybrid zero dynamics [19] optimization problem. This combined approach was first developed in [20], [35]. Here we extend it to generate gaits with subject-specific motion capture data and realize these walking gaits on 2 subjects through an online CLF optimization-based controller.

Separable Output Construction. We define the outputs as,

$$y_v(x) = y_v^a(x) - y_v^d(\tau_v(x), \alpha_v),$$

where y_v^a is the actual output of \mathcal{D}_v and y_v^d is the desired output given by a Bézier polynomial defined by parameters α_v and modulated by a state-based phase variable:

$$\tau_v(x) = \frac{\delta_v(x) - \delta_v^0}{\delta_v^f - \delta^0}.$$

Here $\delta_v(x)$ is a function of the states that monotonically increases from δ_v^0 to δ_v^f during a domain.

To develop a controller for the subsystem (5), we select separable outputs $y_v(x) = (y_v^{rT}(x), y_v^{sT}(x_s))^T$, such that outputs for the subsystem $y_v^s(x_s)$ and their Lie derivatives [36] do not require information about the remaining system [24]. We define the following separable subsystem outputs:

$$y_{s,v}^{a}(x_s)|_{v \in \{rhs, rhl, lhs, ltl, lhl\}} = [\theta_{pk}, \theta_{pa}]^T,$$
$$y_{s,rts}^{a}(x_s) = [v_{rhip}, \theta_{pk}]^T,$$

with,

$$v_{rhip}(x_s) = (\bar{r}_B + r_{pk})\dot{\theta}_{pk} + (\bar{r}_B + r_{pa})\dot{\theta}_{pa},$$

where r_{\square} is the length between the joint specified in the subscript and the following distal joint, and \bar{r}_B is the length between the prosthesis base frame and the prosthesis knee.

To do state-based control for the first 4 domains, we define,

$$\begin{split} \delta_{rhs}(x_s) &= \bar{\theta}_{By}, \\ \delta_{v}(x_s)|_{v \in \{rts, rhl, lhs\}} &= \bar{r}_B \bar{\theta}_{By} + r_{pk} \theta_{pk} + r_{pa} \theta_{pa}. \end{split}$$

For \mathcal{D}_{lts} and \mathcal{D}_{lhl} we calculate τ_v based on the current time and predicted time duration from trajectory generation.

Human Walking Data. We used the average human relative joint trajectories from the motion capture data set of [37]. For each of our subjects, we selected a data set obtained with subjects with similar height and mass. To divide the data into segments for each domain, we used gait cycle percentage estimates of walking phases from [38]. For each segment of data for a given domain, we fit Bézier polynomials to the data using fit in MATLAB. Since there is not an impact causing discrete dynamics between the ts and hl domains, we used a single Bézier stretched across both domains. This process gave a set of Bézier coefficients α_n^H for each domain.

Hybrid Zero Dynamics Optimization. To generate desired trajectories similar to the Bézier polynomials fit to human data that are also provably stable for our prosthesis model, we constructed a human model with computed parameters, as described in II, for each subject. To guarantee stability for these models, we construct a constraint for our hybrid system. In the continuous dynamics of each domain, \mathcal{D}_v , we drive our outputs to 0 through the control input u_v . This reduces the system to a lower dimensional manifold called the partial hybrid zero dynamics (PHZD) surface (or hybrid zero dynamics surface in domains without a velocity modulating output) [35]:

$$\mathbf{PZ}_{\alpha_v} = \{x \in \mathcal{D}_v : y_{2,v}(x,\alpha_v) = 0, \dot{y}_{2,v}(x,\alpha_v) = 0\}.$$

The control input u_v only guarantees PHZD for \mathcal{D}_v . To guarantee PHZD for the entire multi-domain hybrid system, we require the PHZD surface remain invariant through impact, mathematically expressed as,

$$\Delta_e(S_e \cap \mathbf{PZ}_{\alpha_v}) \subseteq \mathbf{PZ}_{\alpha_{v+1}}$$
.

To find parameters α_v that define desired trajectories that both match human data and satisfy this invariant condition, we formulate the following optimization:

$$c_v^{\star} = \operatorname{argmin} \sum_{i=1}^{6} w_i (\theta_i^j - \mathbf{B}(\alpha_{v,i}^H, \tau_v(x))^2 + u_v^T u_v$$
s.t. $\Delta_e(S_e \cap \mathbf{PZ}_{\alpha_v}) \subseteq \mathbf{PZ}_{\alpha_{v+1}}$

physical constraints

$$c_v^{\star} = (\alpha_v^{\star T}, v_{hip,v}^{d\star}, \delta_v^{0\star}, \delta_v^{f,\star})^T.$$

Here we minimize the difference between the joint states $\theta^j = (\theta_{lh}, \theta_{lk}, \theta_{la}, \theta_{rh}, \theta_{pk}, \theta_{pa})^T$ and the Bézier fit $\mathbf{B}(\alpha_{v,i}^H, \tau_v(x))$ of human joint data evaluated at the phase variable. We simultaneously minimize the torque to reduce the energy expenditure and generate smoother torque profiles. We include other physical constraints such as holonomic constraints, virtual constraints (outputs), and decision variable bounds. The solution to the optimization c_v^\star gives parameters α_v^\star to define our desired trajectories, desired hip velocity $v_{hip,v}^d$, and phase variable parameters $\delta_v^{0\star}$ and $\delta_v^{f\star}$ for each domain. We solve this nonlinear hybrid optimization problem through FROST software [39].

IV. CONTROLLER REALIZATION

To enforce these trajectories on the prosthesis subsystem, we employ a rapidly exponentially stabilizing CLF (RES-CLF), following the construction method in [17].

Subsystem RES-CLF. We differentiate the outputs,

$$\begin{bmatrix} \dot{y}_{1,v}^{s} \\ \dot{y}_{2,v}^{s} \end{bmatrix} = \underbrace{\begin{bmatrix} L_{\bar{f}_{v}^{s}} y_{1,v}^{s} \\ L_{\bar{f}_{v}^{s}}^{2} y_{2,v}^{s} \end{bmatrix}}_{L_{\bar{f}_{v}^{s}} y_{v}^{s}} + \underbrace{\begin{bmatrix} L_{\bar{g}_{v}^{s}} y_{1,v}^{s} \\ L_{\bar{g}_{v}^{s}} L_{\bar{f}_{v}^{s}} y_{2,v}^{s} \end{bmatrix}}_{\bar{A}_{v}} u_{s}, \tag{6}$$

with Lie derivatives in $L_{\bar{f}_v^s}y_v^s$ and \bar{A}_v . Here \bar{A}_v is invertible because the outputs are linearly independent, making the system feedback linearizable [36] with the control law,

$$u_s(\mathcal{X}) = \bar{A}_v^{-1}(-L_{\bar{f}^s}y_v^s + \nu).$$
 (7)

Here ν is an auxiliary control input a user can select to stabilize the linearized system, which takes this form with coordinates $\xi = (y_1^{sT}, y_2^{sT}, \dot{y}_2^{sT})^T$,

$$\dot{\xi} = \underbrace{\begin{bmatrix} 0 & 0 & 0 \\ 0 & 0 & \mathbf{I} \\ 0 & 0 & 0 \end{bmatrix}}_{F} \xi \underbrace{\begin{bmatrix} \mathbf{I} & 0 \\ 0 & 0 \\ 0 & \mathbf{I} \end{bmatrix}}_{C} \nu.$$

For this linear system and weighting matrix $Q = Q^T > 1$, we solve the continuous time algebraic Riccati equation for solution $P = P^T > 0$ to construct a RES-CLF:

$$V(\xi) = \xi^T \underbrace{\mathbf{I}_{\varepsilon} P \mathbf{I}_{\varepsilon}}_{P} \xi, \quad \text{with } \mathbf{I}_{\varepsilon} := \text{diag}(\mathbf{I}, \frac{1}{\varepsilon} \mathbf{I}, \mathbf{I}).$$

Taking the derivative yields the convergence constraint:

$$\dot{V}(\xi,\nu) = L_F V(\xi) + L_G V(\xi) \nu \le -\frac{1}{\varepsilon} \frac{\lambda_{min}(Q)}{\lambda_{max}(P)} V(\xi),$$

with Lie derivatives along the linearized output dynamics,

$$L_F V(\xi) = \xi^T (F^T P_{\varepsilon} + P_{\varepsilon} F) \xi,$$

$$L_G V(\xi) = 2 \xi^T P_{\varepsilon} G.$$

Force Sensing ID-CLF-QP. To develop a hardware implementable form of a RES-CLF, we construct a variation of the inverse dynamics CLF QP (ID-CLF-QP), introduced in [23], that was developed for the prosthesis subsystem in [27]. To prescribe a desired behavior to our output dynamics $(\dot{y}_{1,v}^{sT}, \ddot{y}_{2,v}^{sT}) = \nu$, we define a desired auxiliary control input,

$$\nu_{\mathrm{pd}} := K_p y_{2,v}^s(x_s) + K_d \dot{y}_{2,v}^s(x_s) + K_{y^a} \dot{y}_{2,v}^{s,a}(x_s) + K_v y_{1,v}^s(x_s).$$

We added the $K_{y^a}\dot{y}_{2,v}^{s,a}(x_s)$ to the typical output PD law [17], [23] to reduce oscillations observed on hardware. In our QP cost we will minimize the difference between our actual auxiliary control input ν and $\nu_{\rm pd}$. If we solved (7) for ν , the expression would involve computationally expensive matrix inversions prone to numerical error [23]. Instead we use $\nu=(\dot{y}_{1,v}^{sT},\ddot{y}_{2,v}^{sT})^T$ and rewrite our outputs in terms of the subsystem configuration coordinates \bar{q} and velocities \bar{q} :

$$\begin{bmatrix} \dot{y}_{1,v}^{s} \\ \ddot{y}_{2,v}^{s} \end{bmatrix} = \underbrace{\begin{bmatrix} \frac{\partial y_{1,v}^{s}}{\partial \bar{q}} \\ \frac{\partial}{\partial \bar{q}} \left(\frac{\partial y_{2,v}^{s}}{\partial \bar{q}} \dot{\bar{q}} \right) \end{bmatrix}}_{\dot{J}_{y}(\bar{q},\bar{q})} \dot{\bar{q}} + \underbrace{\begin{bmatrix} \frac{\partial y_{1,v}^{s}}{\partial \dot{q}} \\ \frac{\partial y_{s}}{\partial \bar{q}} \end{bmatrix}}_{J_{y}(\bar{q})} \ddot{\bar{q}}.$$

We will include these terms in the QP cost with the holonomic constraints, enforcing these as soft constraints, using,

$$J_c(\bar{q}) = \begin{bmatrix} J_y(\bar{q}) \\ \bar{J}_h(\bar{q}) \end{bmatrix}, \qquad \dot{J}_c(\bar{q}, \dot{q}) = \begin{bmatrix} \dot{J}_y(\bar{q}, \dot{\bar{q}}) \\ \dot{J}_h(\bar{q}, \dot{\bar{q}}) \end{bmatrix}.$$

With these terms, we formulate our ID-CLF-QP,

$$\Upsilon_{v}^{\star} = \underset{\Upsilon \in \mathbb{R}^{n_{v}}}{\operatorname{argmin}} \left\| \dot{J}_{c,v}(\bar{q}, \dot{\bar{q}}) \dot{\bar{q}} + J_{c,v}(\bar{q}) \ddot{\bar{q}} - \mu \right\|^{2} + \sigma W(\Upsilon) + \rho \zeta$$
s.t.
$$\bar{D}(\bar{q}) \ddot{\bar{q}} + \bar{H}(\bar{q}, \dot{\bar{q}}) = \bar{B}_{v} u_{s,v} + \bar{J}_{h,v}^{T}(\bar{q}) \tilde{F}_{g,v} + \bar{J}_{f}^{T}(\bar{q}) F_{f}$$

$$L_{F} V_{v}(\mathcal{X}) + L_{G} V_{v}(\mathcal{X}) (\dot{J}_{y,v} \dot{\bar{q}} + J_{y,v} \ddot{\bar{q}})$$

$$\leq -\frac{1}{\varepsilon} \frac{\lambda_{min}(Q)}{\lambda_{max}} V_{v}(\mathcal{X}) + \rho$$

$$- u_{\max} \leq u_{s,v} \leq u_{\max},$$
(8)

with decision variables $\tilde{\Upsilon}_v = (\ddot{q}^T, u_{s,v}^T, \bar{\lambda}_{h,x,v}, \zeta)^T$. Here $\mu^{\mathrm{pd}} = (\nu_{\mathrm{pd}}^T, 0^T)^T$, $W(\Upsilon)$ is a regularization term to make the system well-posed, σ and ρ are user-selected weights, and ζ is a relaxation term to allow the torque bounds $(-u_{\mathrm{max}}, u_{\mathrm{max}})$ to be met. (We omit the arguments of J_y, \dot{J}_y for notational simplicity.) The GRFs $\tilde{F}_{g,v}$ contain the GRFs present for \mathcal{D}_v . We obtain the vertical GRF $F_{g,z}$ and pitch moment $M_{g,y}$ from a pressure sensor and the QP solves for x-component of the holonomic constraint $\bar{\lambda}_{h,x}$. Even though

the desired auxiliary control law $\nu_{\rm pd}$ differs from that which guarantees stability of the linearized system (6), we still have stability guarantees since the QP selects values that satisfy the CLF constraint. The dimensions and components of this controller are domain-dependent since the outputs and contact points change with domain. We apply and compute GRFs respective to the domain's contact points.

V. EXPERIMENTAL RESULTS

We realize this model and force-based multi-domain controller on our powered prosthesis platform for 2 subjects, resulting in human-like multi-contact behavior.

Prosthesis Platform. We implement the ID-CLF-QP (8) on the powered prosthesis platform AMPRO3 [32], Fig. 3. This platform consists of two brushless DC motors (MOOG BN23) coupled with pulley systems and harmonic gear boxes. These motors are controlled with ELMO motion controllers (Gold Solo Whistle) which obtain joint position and velocity measurements from incremental encoders. The motor controllers send this feedback to the microprocessor, a Beaglebone Black Rev C (BBB), which returns a commanded torque. The controller algorithm is coded in C++ and ROS and runs at 111 Hz on the BBB.

A SensorProd Inc. Tactilus Insole Sensor System, High-Performance V Series (SP049) is placed inside the prosthesis shoe to measure GRFs. An UP Board (2/32) scans the pressure sensors readings and sends the measurements to the BBB. A 6-axis load cell (M3564F, Sunrise Instruments) connects the distal end of the iWalk human adapter to the proximal end of the prosthesis such that it measures the forces the human exerts on the prosthesis through the adapter. The load cell signals go through its signal conditioning box (M8131) and then to the BBB. A Yost Labs 3-SpaceTM Sensor USB/RS232 IMU is mounted to the iWalk to measure the global rotation and velocity of the human's thigh and connects to the BBB. Everything is powered by a Zippy 4000mAh 10S LiPo battery pack. The whole system weighs 10.54 kg, while the prosthesis on its own weighs 5.95kg. For more details on the platform, see [32], and for the force sensors and IMU, [27].

Experimental Set-up. Two non-amputee subjects wore the prosthesis device through an iWalk adapter. Subject 1 was a 1.7 m, 66 kg female and Subject 2 was a 1.8 m 75 kg male. Both subjects wore a shoe lift on their left leg to even out the limb length difference caused by the prosthesis. The subjects were allowed a chance to walk with the device before data recording started. Then they walked with each of the 3 controllers for at least 4 sets of 8 step cycles, taking a short break between controllers. The controllers included the ID-CLF-QP with force sensing (8) ("sensor" controller), the ID-CLF-QP with no force sensing ("no sensor" controller), and a PD controller ¹. When no force sensing was used, all of

¹A small mechanical issue was present in the PD controller test with Subject 2. Because the tracking results were comparable to the PD controller test with Subject 1 we consider the effect of the mechanical issue to be minor and included the results for completeness.

TABLE I
TRACKING RMSE DURING ALL DOMAINS

	Knee RMSE (rad)		Ankle RMSE (rad)	
	Subject 1	Subject 2	Subject 1	Subject 2
Sensor	0.0228	0.0230	0.0179	0.0150
No Sensor	0.0334	0.0315	0.0270	0.0306
PD Control	0.0242	0.0250	0.0494	0.0316

TABLE II
TRACKING RMSE DURING WEIGHT-BEARING DOMAINS

	Knee RMSE (rad)		Ankle RMSE (rad)	
	Subject 1	Subject 2	Subject 1	Subject 2
Sensor	0.0215	0.0276	0.0204	0.0197
No Sensor	0.0429	0.0420	0.0361	0.0432
PD Control	0.0334	0.0344	0.0606	0.0436

the GRFs were calculated through the holonomic constraints in the ID-CLF-QP. The weights and regularization terms in the ID-CLF-QP and the gains in $\nu_{\rm pd}$ were kept consistent for all tests. We set $v_{hip,v}^d=0$ to allow the human to dictate the velocity of their stance progression instead of prescribing a set velocity. We also switched the phase variable from state-based to time-based during \mathcal{D}_{lhs} if the ground contact guard condition was met before τ reached 1 since the state-based phase variable would not progress as expected once the prosthesis foot lifted off of the ground. This also ensured the controller reached the end of the desired trajectory segment for that domain before transitioning to the next domain to maintain continuity of the desired trajectory.

Experimental Results. The supplemental video shows the experiments [40]. Note that the subjects held onto the iWalk adapter with their hand to aid their balance since handrails were not present and there was asymmetry between their legs. Fig. 4 shows the phase portraits of the prosthesis joints for 8 continuous step cycles with the ID-CLF-QP (8). The velocity varies between steps since the desired trajectories are modulated by a state-based phase variable and because the phase variable sometimes switches to time-based during \mathcal{D}_{lhs} . This switching causes two distinct periodic orbits to emerge for subject 2. Future work will aim to obtain a more consistent measure of phase.

Fig. 5 (a) shows the vertical GRF and pitch moment measured by the pressure sensor and horizontal GRF calculated by the QP (8) during 1 step of walking with (8). For each controller, we computed the mean of the actual trajectories, for a set of 8 continuous step cycles, and plotted these against the desired trajectories and the subject-specific average human joint data [37] in Fig. 5 (b). Here the ID-CLF-QP with force sensing (8) exhibits tight tracking to the desired trajectory, especially compared to the other controllers for the ankle. This tracking performance is quantified by the rootmean-square error (RMSE) in Table I showing it outperforms the other controllers for both joints and both subjects. This force-sensing controller responds to the user's load, making its benefits even more pronounced in the 4 weight-bearing domains $(\mathcal{D}_{rhs}, \mathcal{D}_{rts}, \mathcal{D}_{rhl}, \mathcal{D}_{lhs})$, shown by the RMSE in Table II. These results demonstrate this ID-CLF-QP with force sensing enables us to realize prescribed human-like joint kinematics in a systematic way that does not involve tuning between subjects.

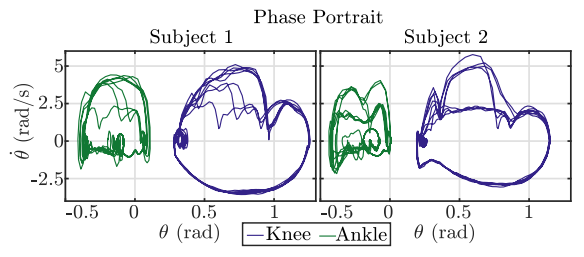


Fig. 4. Phase portraits of the knee and ankle for 2 subjects for 8 continuous steps cycles using the ID-CLF-QP.

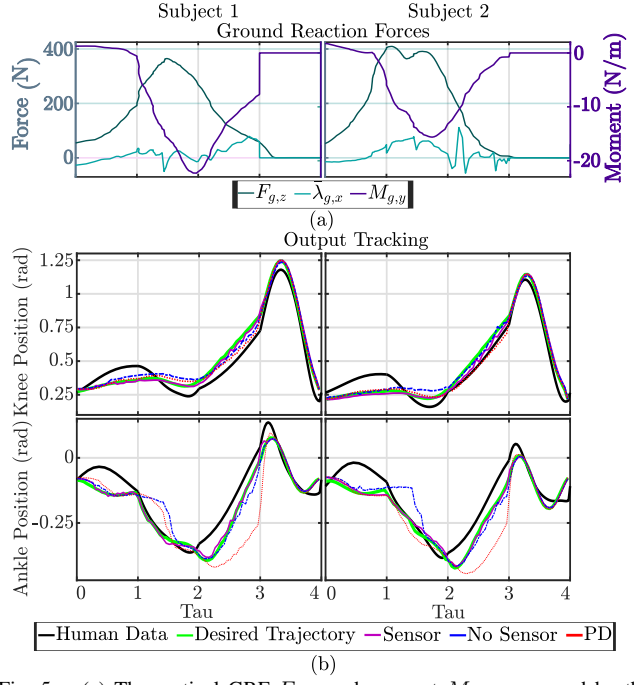


Fig. 5. (a) The vertical GRF $F_{g,z}$ and moment $M_{g,y}$ measured by the pressure sensor and horizontal GRF $\lambda_{g,x}^-$ during one step of walking with the ID-CLF-QP (8). (b) The mean of the actual outputs of the knee and ankle for 2 subjects and 3 controllers for 8 continuous step cycles plotted against the desired trajectory and the averaged human joint data.

VI. CONCLUSION AND FUTURE WORK

This work achieved human-like multi-contact human-prosthesis walking on 2 subjects using a model-based multi-domain controller with real-time force sensing, with no tuning between subjects. This approach provides a formally based, systematic method to generate and realize human-like motion on lower-limb powered prostheses. In terms of tracking, this controller outperformed its counterpart without force sensors and a standard PD controller on both subjects. Being able to realize multi-contact behavior on prostheses without tuning for each subject could bring the benefits of smoother and more energy efficient gait to amputees, restoring natural and healthy locomotion.

While this work was limited to a single trajectory for each subject, this methodology could be extended to realize a variety of behaviors on prostheses by generating a gait library offline, as in [41]. This would expedite the tuning process currently required by impedance control to realize human kinematic trends on powered prostheses. Additionally, using a more realistic human model, that accounts for humans' compliance and variability between steps, could yield more robust and natural locomotion.

REFERENCES

- [1] C. H. Soo and J. M. Donelan, "Mechanics and energetics of step-tostep transitions isolated from human walking," *Journal of Experimental Biology*, vol. 213, no. 24, pp. 4265–4271, 12 2010.
- [2] L. F. Teixeira-Salmela, S. Nadeau, M.-H. Milot, D. Gravel, and L. F. Requião, "Effects of cadence on energy generation and absorption at lower extremity joints during gait," *Clinical Biomechanics*, vol. 23, no. 6, pp. 769–778, 2008.
- [3] V. T. Inman, "Human locomotion." Canadian Medical Association journal, vol. 94 20, pp. 1047–54, 1966.
- [4] V. I. Inman, H. J. Ralston, F. Todd, and J. C. Lieberman, Human Walking, 5th ed. Boca Raton, FL, USA: Williams and Wilkins, 1981.
- [5] A. D. Kuo, "Energetics of Actively Powered Locomotion Using the Simplest Walking Model," *Journal of Biomechanical Engineering*, vol. 124, no. 1, pp. 113–120, 09 2001.
- [6] D. Morgenroth, A. Segal, K. Zelik, J. Czerniecki, G. Klute, P. Adamczyk, M. Orendurff, M. Hahn, S. Collins, and A. Kuo, "The effect of prosthetic push-off on mechanical loading associated with knee osteoarthritis in lower extremity amputees," *Gait & posture*, vol. 34, pp. 502–7, 07 2011.
- [7] P. DeVita, J. Helseth, and T. Hortobagyi, "Muscles do more positive than negative work in human locomotion," *The Journal of experimental* biology, vol. 210, pp. 3361–73, 10 2007.
- [8] R. L. Waters and S. Mulroy, "The energy expenditure of normal and pathologic gait," *Gait & Posture*, vol. 9, no. 3, pp. 207–231, 1999.
- [9] R. Gailey, "Review of secondary physical conditions associated with lower-limb amputation and long-term prosthesis use," *The Journal of Rehabilitation Research and Development*, vol. 45, no. 1, pp. 15–30, dec 2008.
- [10] F. Sup, A. Bohara, and M. Goldfarb, "Design and control of a powered transfemoral prosthesis," *The International Journal of Robotics Research*, vol. 27, no. 2, pp. 263–273, 2008, pMID: 19898683.
- [11] B. E. Lawson, H. A. Varol, A. Huff, E. Erdemir, and M. Goldfarb, "Control of stair ascent and descent with a powered transfemoral prosthesis," *IEEE Transactions on Neural Systems and Rehabilitation Engineering*, vol. 21, no. 3, pp. 466–473, 2013.
- [12] K. Bhakta, J. Camargo, P. Kunapuli, L. Childers, and A. Young, "Impedance Control Strategies for Enhancing Sloped and Level Walking Capabilities for Individuals with Transfemoral Amputation Using a Powered Multi-Joint Prosthesis," *Military Medicine*, vol. 185, no. Supplement 1, pp. 490–499, 12 2019.
- [13] A. Simon, K. Ingraham, N. Fey, S. Finucane, R. Lipschutz, A. Young, and L. Hargrove, "Configuring a powered knee and ankle prosthesis for transfemoral amputees within five specific ambulation modes," *PloS one*, vol. 9, p. e99387, 06 2014.
- [14] B. E. Lawson, J. Mitchell, D. Truex, A. Shultz, E. Ledoux, and M. Goldfarb, "A robotic leg prosthesis: Design, control, and implementation," *IEEE Robotics & Automation Magazine*, vol. 21, no. 4, pp. 70–81, 2014.
- [15] K. Ziegler-Graham, E. J. MacKenzie, P. L. Ephraim, T. G. Travison, and R. Brookmeyer, "Estimating the prevalence of limb loss in the united states: 2005 to 2050," *Archives of Physical Medicine and Rehabilitation*, vol. 89, no. 3, pp. 422–429, 2008.
- [16] K. Sreenath, H.-W. Park, I. Poulakakis, and J. W. Grizzle, "A compliant hybrid zero dynamics controller for stable, efficient and fast bipedal walking on mabel," *The International Journal of Robotics Research*, vol. 30, no. 9, pp. 1170–1193, 2011.
- [17] A. D. Ames, K. Galloway, K. Sreenath, and J. W. Grizzle, "Rapidly exponentially stabilizing control Lyapunov functions and hybrid zero dynamics," *IEEE Transactions on Automatic Control*, vol. 59, no. 4, pp. 876–891, 2014.
- [18] J. P. Reher, A. Hereid, S. Kolathaya, C. M. Hubicki, and A. D. Ames, Algorithmic Foundations of Realizing Multi-Contact Locomotion on the Humanoid Robot DURUS. Cham: Springer International Publishing, 2020, pp. 400–415.
- [19] E. R. Westervelt, J. W. Grizzle, C. Chevallereau, J. H. Choi, and B. Morris, Feedback control of dynamic bipedal robot locomotion. CRC press, 2018.

- [20] H. Zhao, A. Hereid, W.-l. Ma, and A. D. Ames, "Multi-contact bipedal robotic locomotion," *Robotica*, vol. 35, no. 5, p. 1072–1106, 2017.
- [21] H. Zhao, J. Horn, J. Reher, V. Paredes, and A. D. Ames, "Multicontact locomotion on transfemoral prostheses via hybrid system models and optimization-based control," *IEEE Transactions on Automation* 2012, 1971, 2012.
- Science and Engineering, vol. 13, no. 2, pp. 502–513, April 2016. [22] K. Galloway, K. Sreenath, A. D. Ames, and J. W. Grizzle, "Torque saturation in bipedal robotic walking through control lyapunov function-based quadratic programs," *IEEE Access*, vol. 3, pp. 323–332, 2015.
- [23] J. Reher, C. Kann, and A. D. Ames, "An inverse dynamics approach to control lyapunov functions," in 2020 American Control Conference (ACC), 2020, pp. 2444–2451.
- [24] R. Gehlhar, J. Reher, and A. D. Ames, "Control of separable subsystems with application to prostheses," arXiv preprint arXiv:1909.03102, 2019.
- [25] A. E. Martin and R. D. Gregg, "Stable, robust hybrid zero dynamics control of powered lower-limb prostheses," *IEEE Transactions on Automatic Control*, vol. 62, no. 8, pp. 3930–3942, 2017.
- [26] R. Gehlhar and A. D. Ames, "Separable control lyapunov functions with application to prostheses," *IEEE Control Systems Letters*, vol. 5, no. 2, pp. 559–564, 2021.
- [27] R. Gehlhar, J.-h. Yang, and A. D. Ames, "Powered prosthesis locomotion on varying terrains: Model-dependent control with real-time force sensing," *IEEE Robotics and Automation Letters*, vol. 7, no. 2, pp. 5151–5158, 2022.
- [28] A. D. Ames, R. Vasudevan, and R. Bajcsy, "Human-data based cost of bipedal robotic walking," in *Proceedings of the 14th International Conference on Hybrid Systems: Computation and Control*, ser. HSCC '11. New York, NY, USA: Association for Computing Machinery, 2011, p. 153–162.
- [29] R. M. Murray, S. S. Sastry, and L. Zexiang, A Mathematical Introduction to Robotic Manipulation, 1st ed. Boca Raton, FL, USA: CRC Press, Inc., 1994.
- [30] S. Plagenhoef, F. G. Evans, and T. Abdelnour, "Anatomical data for analyzing human motion," *Research Quarterly for Exercise and Sport*, vol. 54, no. 2, pp. 169–178, 1983.
- [31] W. Erdmann, "Geometry and inertia of the human body review of research," Acta of Bioengineering and Biomechanics, vol. 1, pp. 23– 35, 1999.
- [32] H. Zhao, E. Ambrose, and A. D. Ames, "Preliminary results on energy efficient 3D prosthetic walking with a powered compliant transfemoral prosthesis," in *Robotics and Automation (ICRA)*, 2017 IEEE International Conference on. IEEE, 2017, pp. 1140–1147.
- [33] G. Andréasson and L. Peterson, "Effects of shoe and surface characteristics on lower limb injuries in sports," *International Journal of Sport Biomechanics*, vol. 2, no. 3, pp. 202 209, 1986.
- [34] H. Zhao, A. Hereid, E. Ambrose, and A. D. Ames, "3d multi-contact gait design for prostheses: Hybrid system models, virtual constraints and two-step direct collocation," in 2016 IEEE 55th Conference on Decision and Control (CDC), 2016, pp. 3668–3674.
- [35] A. D. Ames, "Human-inspired control of bipedal walking robots," IEEE Transactions on Automatic Control, vol. 59, no. 5, pp. 1115– 1130, 2014.
- [36] A. Isidori, Nonlinear Control Systems. Springer London, 1995.
- [37] J. Camargo, A. Ramanathan, W. Flanagan, and A. Young, "A comprehensive, open-source dataset of lower limb biomechanics in multiple conditions of stairs, ramps, and level-ground ambulation and transitions," *Journal of Biomechanics*, p. 110320, 2021.
- [38] J. Perry and J. M. Burnfield, Gait Analysis: Normal and Pathological Function, 2nd ed. New York, NY, USA: Slack Incorporated, 2010.
- [39] A. Hereid, E. A. Cousineau, C. M. Hubicki, and A. D. Ames, "3D dynamic walking with underactuated humanoid robots: A direct collocation framework for optimizing hybrid zero dynamics," in *Robotics and Automation (ICRA)*, 2016 IEEE International Conference on. IEEE, 2016, pp. 1447–1454.
- [40] https://youtu.be/gdYcPq3Si18.
- [41] J. Reher and A. D. Ames, "A control lyapunov function-based controller for compliant hybrid zero dynamic walking on cassie," submitted to IEEE Transactions on Robotics (T-RO), 2021 (In Preparation).